Robust Deadbeat Predictive Power Control with a Discrete-time Disturbance Observer for PWM Rectifiers under Unbalanced Grid Conditions

Haitao Yang, *Student Member, IEEE,* Yongchang Zhang, *Member, IEEE,* Jiejunyi Liang, Jie Liu, Nong Zhang and Paul D. Walker

Haitao Yang, Jiejunyi Liang, Nong Zhang and Paul D. Walker are with School of Electrical, Mechanical and Mechatronic Sytstems, University of Technology Sydney, Australia.

Yongchang Zhang and Jie Liu are with Power Electronics and Motor Drives Engineering Research Center of Beijing, North China University of Technology, Beijing, China.

Abstract

This paper presents a robust deadbeat predictive power control (DPPC) for PWM rectifiers with consideration of parameter mismatches under unbalanced grid conditions. Firstly, conventional DPPC is modified to extend its application to both ideal and unbalanced grid conditions. Secondly, tracking error of the modified DPPC with inaccurate grid-side impedance is analyzed. Thirdly, a discrete-time power disturbance observer (DPDO) is designed to achieve accurate power control with mismatched parameters. The designed DPDO can predict complex power at the next sampling instant and estimate system disturbance simultaneously. Therefore, the DPDO can contribute to eliminate steady-state tracking error resulting from disturbances caused by inaccurate parameters and compensate one-step delay in digital implementation. Although satisfactory steady-state performance can be obtained with modified DPPC and DPDO, transient performance still deteriorates significantly with inaccurate value of grid-side inductance. Thus, an online adaptive method to estimate mismatched inductance is finally developed based on the proposed DPDO. Both DPPC and DPDO are implemented in the stationary reference frame without coordinate transformation. Theoretical analysis confirms that the proposed DPDO can track disturbance without phase lag or magnitude error. Experimental tests and comparative studies with a prior DPPC on a two-level PWM rectifier validate the effectiveness of the proposed scheme.

Index Terms

Predictive control, PWM rectifiers, parameter estimation, unbalanced grid

I. Introduction

Three phase voltage source PWM rectifiers (VSR) have been widely used in various applications [1], [2]. To control the power flow of VSR, voltage oriented control (VOC) [3], [4], direct power control (DPC) [5], [6], model

Corresponding author: Yongchang Zhang. Tel.:+86-10-88803922-204. E-mail:zhangdavid37@gmail.com.

Part of this paper was presented at the IEEE Energy Conversion Congress and Exposition, Cincinnati, OHIO, USA, 2017, see [32].

predictive control [7], [8], etc. have been proposed.

VOC has advantages of satisfactory steady-state performance and fixed switching frequency. However, to prevent high overshoot and reduce the sensitivity to noise, it is difficult to achieve fast dynamic responses by VOC using conventional proportional-integral controllers [9]. DPC utilizes two hysteresis controllers to control active power and reactive power. Fast power response, simplicity for implementation and good robustness against parameter variation are usually considered as the main virtues of DPC. However, large power ripples, high sampling frequency and variable switching frequency are limitations that need to be solved [10]. Recently, finite control-set model predictive control (FCS-MPC) has attracted wide attention due to quick dynamic responses, satisfactory steady-state performance and simplicity of handling state constraints [1], [11]. As FCS-MPC is a model based control scheme, the variation of parameters would inevitably cause performance deterioration [12] and FCS-MPC has drawbacks of the requirement of fast sampling frequency and high computational burden, especially for a long prediction horizon in practical application.

Apart from FCS-MPC, deadbeat control (DBC) is another form of model based predictive control. This method has been widely used in the current control [13], [14], torque control [15], [16] and power control [17], [18] for motor drives and converters. In [10], a space vector modulation (SVM) based deadbeat predictive power control (DPPC) is investigated. Then, it is extended in [18] using a new definition of reactive power to eliminate active power ripples while maintaining sinusoidal grid currents under unbalanced grid voltages. The merits of DPPC includes constant switching frequency, no need to use phase-locked-loop (PLL) and fast dynamic response. However, as DPPC is derived based on inverse model of the system, exact model parameters are required to obtain an accurate control signal. If parameter mismatches exist, the calculated control signal can not force the concerned state variables to reach their references.

To address deteriorated control performance caused by parameter mismatches for predictive control, different online correction methods can be found in literature. In [19], the effects of model uncertainty is studied and then a least squares estimation is designed to update model parameters. In [20], the grid-side inductance is estimated by comparing magnitudes of calculated grid voltages within two sampling periods. However, since magnitude of grid voltage vector is not a constant for unbalanced three-phase voltages, this method cannot be directly applied to unbalanced networks. Other techniques, such as evaluating tracking error of reactive power [21] and injecting test signals [22] can also be employed to get actual model parameters. Apart from parameter adaption, disturbance observers are also employed in many studies to improve control accuracy. A Luenberger observer is designed in [13] and [23] to improve robustness of predictive control. Both schemes are implemented in synchronous reference frame. A proportional–integral observer is proposed in [24] for one-step ahead predictor without offset during steady-state operation. Since integrator can not track AC disturbances without phase lag and magnitude error, this scheme should be implemented in synchronous reference frame as that in [13] for three-phase VSRs. For those control schemes implemented in stationary reference frame (e.g. DPPCs in [10] and [18]), it is preferable to design a disturbance observer in stationary reference frame.

For deadbeat control of power converters, both current vector and complex power can be selected as control variable. In most previous research [13], [24]–[26], disturbance observers are designed based on measured current.

Few have considered a disturbance observer constructed based on the complex power. What's more, they are usually designed assuming an ideal grid. Hence, their feasibility in unbalanced grid conditions needs to be further verified. As these disturbance observers are usually implemented in the synchronous reference frame, they can not be simply integrated into control schemes implemented in stationary reference frame. There are some observers designed for unbalanced network, such as those presented in [27]–[29]. However, they are usually used for estimating or predicting fundamental and harmonic components of grid voltages. Using an observer to estimate disturbances caused by mismatched parameters under unbalanced grid conditions in stationary reference frame still needs to be investigated.

In practical application, it is necessary to ensure that PWM rectifier could properly work under both ideal and unbalanced grid conditions. For a weak grid, unbalanced grid condition with 15% single-phase voltage sag is very common [30]. Considering severely unbalanced conditions may occur due to grid fault, highly imbalanced load, etc., more severe voltage sag such as 50% and 90% voltage dips in single-phase are experimentally investigated in [31]. In this paper, the disturbance observer and DPPC presented in [32] which can only work properly under ideal grid conditions are revised to extend their application under unbalanced grid conditions. In [32], the DPDO is designed and analyzed in continuous-time domain with subsequent discretization for practical implementation. In this paper, the DPDO is developed in the discrete-time domain for the three-phase three-wire converter system. As the discrete nature of the digital controller is directly considered in the design phase, more accurate analytical results and simplified implementation process are achieved. Furthermore, the guidelines for choosing observer parameters are developed, and an online adaptive method for inductance estimation is proposed to further improve the dynamic performance. For the proposed DPDO based DPPC, the estimation of disturbances caused by mismatched parameters is integrated into one-step ahead prediction procedure. As such, one-step delay compensation and disturbance estimation can be achieved simultaneously. Therefore, the proposed scheme would not substantially increase complexity compared to a standard DPPC. Experimental results and comparative research with a prior method [18] justify the effectiveness of the proposed method.

II. Dynamic Equations of VSR

For a three-phase three-wire PWM rectifier, its mathematical model in the stationary $\alpha\beta$ reference frame can be expressed in the complex vector form as

$$L_g \frac{d\boldsymbol{i}_g}{dt} = \boldsymbol{u}_g - \boldsymbol{u}_c - R_g \boldsymbol{i}_g \tag{1}$$

where $\boldsymbol{u}_g = u_{g\alpha} + ju_{g\beta}$, $\boldsymbol{u}_c = u_{c\alpha} + ju_{c\beta}$ and $\boldsymbol{i}_g = i_{g\alpha} + ji_{g\beta}$ are grid voltage vector, converter voltage vector and grid current vector respectively; L_g and R_g are inductance and resistance of grid-side filter. The grid-side complex power $\boldsymbol{S}$ can be calculated as

$$\boldsymbol{S} = P + jQ = 1.5\boldsymbol{i}_g^* \boldsymbol{u}_g. \tag{2}$$

where, P and Q are active power and reactive power; superscript $*$ denotes the conjugate of a complex vector.

For unbalanced grid voltages, $\boldsymbol{u}_g$ can be decomposed into fundamental positive sequence component (FPSC) $\boldsymbol{u}_{gp}$ and fundamental negative sequence component (FNSC) $\boldsymbol{u}_{gn}$ as

$$\boldsymbol{u}_g = \boldsymbol{u}_{gp} + \boldsymbol{u}_{gn}. \tag{3}$$

The zero-sequence component is omitted in (3), because it has no effect on power control for a three-phase three-wire converter system [31]. Similarly, grid current $\boldsymbol{i}_g$ can be written as

$$\boldsymbol{i}_g = \boldsymbol{i}_{gp} + \boldsymbol{i}_{gn}. \tag{4}$$

With grid voltage in (3) and the current controlled as shown in (4), the instantaneous power can be calculated as

$$\begin{bmatrix} P \\ Q \end{bmatrix} = \begin{bmatrix} \overline{P} + P_c\cos(2\omega_g t) + P_s\sin(2\omega_g t) \\ \overline{Q} + Q_c\cos(2\omega_g t) + Q_s\sin(2\omega_g t) \end{bmatrix} \tag{5}$$

where $\overline{P}$ and $\overline{Q}$ are average value of the active power and reactive power and P_c, P_s and Q_c, Q_s are ripple components of P and Q. As derived in [2], the average value and ripple components of P and Q can be further expressed as

$$\overline{P} = \frac{3}{2}\left(\boldsymbol{i}_{dq}^{+} \odot \boldsymbol{e}_{dq}^{+} + \boldsymbol{i}_{dq}^{-} \odot \boldsymbol{e}_{dq}^{-}\right) \tag{6}$$

$$P_c = \frac{3}{2}\left(\boldsymbol{i}_{dq}^{+} \odot \boldsymbol{e}_{dq}^{-} + \boldsymbol{i}_{dq}^{-} \odot \boldsymbol{e}_{dq}^{+}\right) \tag{7}$$

$$P_s = \frac{3}{2}\left(\boldsymbol{i}_{dq}^{+} \otimes \boldsymbol{e}_{dq}^{-} - \boldsymbol{i}_{dq}^{-} \otimes \boldsymbol{e}_{dq}^{+}\right) \tag{8}$$

$$\overline{Q} = \frac{3}{2}\left(\boldsymbol{i}_{dq}^{+} \otimes \boldsymbol{e}_{dq}^{+} + \boldsymbol{i}_{dq}^{-} \otimes \boldsymbol{e}_{dq}^{-}\right) \tag{9}$$

$$Q_c = \frac{3}{2}\left(\boldsymbol{i}_{dq}^{+} \otimes \boldsymbol{e}_{dq}^{-} + \boldsymbol{i}_{dq}^{-} \otimes \boldsymbol{e}_{dq}^{+}\right) \tag{10}$$

$$Q_s = \frac{3}{2}\left(\boldsymbol{i}_{dq}^{-} \odot \boldsymbol{e}_{dq}^{+} - \boldsymbol{i}_{dq}^{+} \odot \boldsymbol{e}_{dq}^{-}\right) \tag{11}$$

where $\boldsymbol{i}_{dq}^{+}$, $\boldsymbol{e}_{dq}^{+}$ represent FPSCs of grid current and grid voltage in the positive-sequence synchronous reference frame and $\boldsymbol{i}_{dq}^{-}$, $\boldsymbol{e}_{dq}^{-}$ denote FNSCs in the negative-sequence synchronous reference frame. It is clear that there are four controllable freedoms (i_d^{+}, i_d^{-}, i_q^{+} and i_q^{-}). This implies only four control targets can be established [31]. In most applications, the average active power and reactive power are controlled to follow their references, i.e.,

$$\overline{P} = P^{ref} \tag{12}$$

$$\overline{Q} = Q^{ref} \tag{13}$$

The remaining two control functions can be selected as one of the following. 1) Eliminating active power ripples, i.e., $P_c = 0$ and $P_s = 0$. In this case, Q_c and Q_s leave to be uncontrolled and thus reactive power ripples exist under unbalanced grid conditions [2]; 2) Eliminating reactive power ripples, i.e., $Q_c = 0$ and $Q_s = 0$. In this case, P_c and P_s are uncontrolled and thus there are active power ripples. 3) Achieving balanced and sinusoidal input currents, i.e., $i_d^{-} = 0$ and $i_q^{-} = 0$. In this case, only two control freedoms (i_d^{+} and i_q^{+}) are available which can only be used for satisfying (12) and (13). As P_c, P_s and Q_c, Q_s are all uncontrolled, both active power and reactive power exhibit power oscillations if grid voltages are unbalanced [31]. As stated above, all control objectives have

their own merits and drawbacks under unbalanced grid conditions. To ensure a fair comparison with [2] and verify the effectiveness of the proposed DPDO, the same control objective of eliminating active power ripples as [2] is selected in this paper.

The quadrature component of grid voltage vector that lagging actual grid voltage vector by 90° can be expressed as [2]

$$\boldsymbol{u}_g^{'} = -j\boldsymbol{u}_{gp} + j\boldsymbol{u}_{gn}. \tag{14}$$

Based on (3) and (14), the derivative of grid voltage vector can be expressed by

$$\frac{d\boldsymbol{u}_g}{dt} = \frac{d\boldsymbol{u}_{gp}}{dt} + \frac{d\boldsymbol{u}_{gn}}{dt} = j\omega_g\boldsymbol{u}_{gp} - j\omega_g\boldsymbol{u}_{gn} = -\omega_g\left(-j\boldsymbol{u}_{gp} + j\boldsymbol{u}_{gn}\right) = -\omega_g\boldsymbol{u}_g^{'}. \tag{15}$$

With the derivatives of $\boldsymbol{i}_g$ and $\boldsymbol{u}_g$ shown in (1) and (15), the derivative of $\boldsymbol{S}$ can be calculated from (2) as

$$\frac{d\boldsymbol{S}}{dt} = \frac{3}{2}\left(\boldsymbol{u}_g\frac{d\boldsymbol{i}_g^*}{dt} + \boldsymbol{i}_g^*\frac{d\boldsymbol{u}_g}{dt}\right) = \frac{1}{L_g}\left[\frac{3}{2}\left(|\boldsymbol{u}_g|^2 - \boldsymbol{u}_c^*\boldsymbol{u}_g\right) - (R_g + \frac{\omega_g L_g\boldsymbol{u}_g^{'}}{\boldsymbol{u}_g})\cdot\boldsymbol{S}\right]. \tag{16}$$

It should be noted that (16) is valid for both ideal and unbalanced grid conditions. For an ideal grid, $\boldsymbol{u}_g^{'} = -j\boldsymbol{u}_g$ holds. In this case, derivative of complex power is the same as that presented in [18], which is a special case of (16).

With a small sampling period, the simple forward Euler method can be employed to discretize (16). The result is shown in (17).

$$\boldsymbol{S}^{k+1} = \boldsymbol{S}^k + \frac{T_{sc}}{L_g}\left[\frac{3}{2}\left(\left|\boldsymbol{u}_g^k\right|^2 - \left(\boldsymbol{u}_c^k\right)^*\boldsymbol{u}_g^k\right) - (R_g + \omega_g L_g J^k)\cdot\boldsymbol{S}^k\right] \tag{17}$$

where, superscript k represents the variable at kth instant; T_{sc} is the sampling period and $J^k = \left(\boldsymbol{u}_g^{'}\right)^k/\boldsymbol{u}_g^k$.

III. Deadbeat Predictive Power Control

A. Reference Compensation for Unbalanced Grid Voltages

In this paper, the control objectives under unbalanced grid conditions are selected as keeping instantaneous active power constant and grid currents sinusoidal. As stated in [2], this can be achieved by adding an imaginary part to the original reference of complex power. The compensation of power reference can be expressed as follow

$$\boldsymbol{S}^{com} = j\frac{\boldsymbol{u}_g\odot\boldsymbol{u}_g^{'}}{\boldsymbol{u}_g\otimes\boldsymbol{u}_g^{'}}P^{ref} \tag{18}$$

where, $\odot$ and $\otimes$ denote dot product and cross product of two complex vectors respectively; P^{ref} is the reference of active power. Detailed derivation of (18) can be found in [2] and thus it is not repeated here. As $\boldsymbol{u}_g\odot\boldsymbol{u}_g^{'} = 0$ for a ideal grid, $\boldsymbol{S}^{com}$ presents in (18) is suitable for both ideal and unbalanced grid conditions. After calculating $\boldsymbol{S}^{com}$, the reference of complex power can be obtained as

$$\boldsymbol{S}^{ref} = P^{ref} + jQ^{ref} + \boldsymbol{S}^{com}. \tag{19}$$

The reactive power reference Q^{ref} is set as zero in this paper. However, it can be found from (18) and (19) that an oscillating imaginary component would be added to the original power reference if grid voltages are unbalanced.

Hence, after compensation, the reactive power reference oscillates under unbalanced conditions. Substituting (18) into (19), $\boldsymbol{S}^{ref}$ can be further rewritten as

$$\boldsymbol{S}^{ref} = P^{ref}\left(1 + j\frac{\boldsymbol{u}_g \odot \boldsymbol{u}_g^{'}}{\boldsymbol{u}_g \otimes \boldsymbol{u}_g^{'}}\right) \tag{20}$$

$$= jP^{ref}\frac{\left(\boldsymbol{u}_g^{'}\right)^{*}\boldsymbol{u}_g}{\boldsymbol{u}_g \otimes \boldsymbol{u}_g^{'}} \tag{21}$$

B. Influence of Mismatched Parameters On Tracking Accuracy

Assuming $\boldsymbol{S}^{k+1} = \boldsymbol{S}^{ref}$, the converter voltage that forces the complex power to reach its reference at the next sampling period can be obtained from (17) as

$$\boldsymbol{u}_c^k = \boldsymbol{u}_g^k - \frac{2}{3}\left(\frac{(R_g + \omega_g L_g J^k)\boldsymbol{S}^k}{\boldsymbol{u}_g^k}\right)^{*} - \frac{2L_g}{3T_{sc}}\left(\frac{\boldsymbol{S}^{ref} - \boldsymbol{S}^k}{\boldsymbol{u}_g^k}\right)^{*}. \tag{22}$$

One can see that the expression of $\boldsymbol{u}_c^k$ includes parameters of grid-side inductance and resistance, which may vary with time due to saturation, temperature, etc. With mismatched parameters, the actual power would deviate from its reference, reducing the accuracy of power control.

To evaluate the impact of parameter mismatch, the estimated inductance and resistance that used in the controller are defined as

$$\hat{L}_g = L_g - \Delta L \tag{23}$$

$$\hat{R}_g = R_g - \Delta R \tag{24}$$

where ΔL and ΔR are the errors of estimated inductance and resistance respectively. In practical application, $\boldsymbol{u}_c^k$ is calculated with $\hat{L}_g$ and $\hat{R}_g$ as

$$\hat{\boldsymbol{u}}_c^k = \boldsymbol{u}_g^k - \frac{2}{3}\left(\frac{(\hat{R}_g + \omega_g \hat{L}_g J^k)\boldsymbol{S}^k}{\boldsymbol{u}_g^k}\right)^{*} - \frac{2\hat{L}_g}{3T_{sc}}\left(\frac{\boldsymbol{S}^{ref} - \boldsymbol{S}^k}{\boldsymbol{u}_g^k}\right)^{*}. \tag{25}$$

Replacing $\boldsymbol{u}_c^k$ in (17) with the above calculated $\hat{\boldsymbol{u}}_c^k$ yields

$$\boldsymbol{S}^{k+1} = \boldsymbol{S}^k + \frac{T_{sc}}{L_g}\left[-\left((R_g - \hat{R}_g) + \omega_g J^k (L_g - \hat{L}_g)\right)\boldsymbol{S}^k\right] + \frac{\hat{L}_g}{L_g}\left(\boldsymbol{S}^{ref} - \boldsymbol{S}^k\right). \tag{26}$$

With (23) and (24), (26) can be further simplified as

$$\boldsymbol{S}^{k+1} = \frac{(L_g - \Delta L)\boldsymbol{S}^{ref} + \left(\Delta L - T_{sc}(\omega_g \Delta L J^k + \Delta R)\right)\boldsymbol{S}^k}{L_g}. \tag{27}$$

It is clear that if ΔL and ΔR are zero, $\boldsymbol{S}^{k+1}$ equals $\boldsymbol{S}^{ref}$. However, if there is any mismatch, the applied voltage (25) can no longer force $\boldsymbol{S}^{k+1}$ to reach $\boldsymbol{S}^{ref}$. As conventional DPPC is sensitive to parameter variations, a robust DPPC based on disturbance estimation will be proposed in the following text. Since $\boldsymbol{S}^{k+1} \approx \boldsymbol{S}^k$ during steady-state operation, (27) can be further simplified as

$$\boldsymbol{S}^k = \frac{\boldsymbol{S}^{ref}}{1 + \left(\Delta R T_{sc} + \omega_g T_{sc} \Delta L J^k\right)/\hat{L}_g}. \tag{28}$$

In practical application, the grid-side resistance is usually small to reduce power losses. Additionally, the influence of ΔR is multiplied by a small value $T_{sc}/\hat{L}_g$. Hence, influence of ΔR on power control is usually negligible.

IV. Disturbance Estimation in Discrete-time Domain

A. Design of DPDO

According to (17), one-step ahead prediction can be rearranged using the following equation with estimated inductance and resistance as

$$\boldsymbol{S}^{k+1} = \boldsymbol{S}^{k} + \frac{T_{sc}}{\hat{L}_g}\left[\frac{3}{2}\left(\left|\boldsymbol{u}_g^k\right|^2 - \left(\boldsymbol{u}_c^k + \boldsymbol{u}_d^k\right)^* \boldsymbol{u}_g^k\right) - (\hat{R}_g + \omega_g \hat{L}_g J^k)\cdot \boldsymbol{S}^k\right] \tag{29}$$

where $\boldsymbol{u}_d$ is the disturbance voltage that compensates the impact of inaccurate parameters so that the responses of (29) is exactly the same with (17). Subtracting (29) from (17) yields

$$\Delta L \cdot \boldsymbol{S}^{k+1} = \Delta L \cdot \boldsymbol{S}^{k} + \frac{3T_{sc}}{2}\left[\left(\boldsymbol{u}_d^k\right)^* \boldsymbol{u}_g^k - (\Delta R + J^k \omega_g \Delta L)\boldsymbol{S}^k\right]. \tag{30}$$

From (30), $\boldsymbol{u}_d^k$ can be solved as

$$\boldsymbol{u}_d^k = \frac{2}{3}\left(\frac{\Delta L\left(\boldsymbol{S}^{k+1} - \boldsymbol{S}^k\right)}{\boldsymbol{u}_g^k T_{sc}} + \frac{(\Delta R + J^k\omega_g \Delta L)\boldsymbol{S}^k}{\boldsymbol{u}_g^k}\right)^*. \tag{31}$$

Similar to $\boldsymbol{u}_g$, $\boldsymbol{u}_d$ can be decomposed into FPSC $\boldsymbol{u}_{dp}$ and FNSC $\boldsymbol{u}_{dn}$ under unbalanced grid condition. The proof is provided in the Appendix. Under steady state, the dynamics of $\boldsymbol{u}_{dp}$ and $\boldsymbol{u}_{dn}$ can be expressed in the discrete-time domain as

$$\begin{cases} \boldsymbol{u}_{dp}^{k+1} &= e^{j\omega_g T_{sc}}\boldsymbol{u}_{dp}^k \\ \boldsymbol{u}_{dn}^{k+1} &= e^{-j\omega_g T_{sc}}\boldsymbol{u}_{dn}^k \end{cases}. \tag{32}$$

As ΔL and ΔR are unknown, $\boldsymbol{u}_d$ is not directly available. A discrete-time disturbance observer is thus designed based on the system model (29) and (32) as follows.

$$\begin{cases} \hat{\boldsymbol{S}}^{k+1} = \hat{\boldsymbol{S}}^{k} + \frac{T_{sc}}{\hat{L}_g}\left[\frac{3}{2}\left(\left|\boldsymbol{u}_g^k\right|^2 - \left(\boldsymbol{u}_c^k + \hat{\boldsymbol{u}}_d^k + \boldsymbol{u}_o^k\right)^* \boldsymbol{u}_g^k\right) - (\hat{R}_g + \omega_g \hat{L}_g J^k)\cdot \boldsymbol{S}^k\right] & (33.1) \\ \hat{\boldsymbol{u}}_{dp}^{k+1} = e^{j\omega_g T_{sc}}\hat{\boldsymbol{u}}_{dp}^k + \lambda \boldsymbol{u}_o^k & (33.2) \\ \hat{\boldsymbol{u}}_{dn}^{k+1} = e^{-j\omega_g T_{sc}}\hat{\boldsymbol{u}}_{dn}^k + \lambda \boldsymbol{u}_o^k & (33.3) \\ \hat{\boldsymbol{u}}_{d}^{k+1} = \hat{\boldsymbol{u}}_{dp}^{k+1} + \hat{\boldsymbol{u}}_{dn}^{k+1} & (33.4) \end{cases}$$

where $\boldsymbol{u}_o$ is a control function; $\hat{\boldsymbol{u}}_d$ is the estimation of disturbance voltage $\boldsymbol{u}_d$; $\hat{\boldsymbol{u}}_{dp}$ and $\hat{\boldsymbol{u}}_{dn}$ are FPSC and FNSC decomposed from $\hat{\boldsymbol{u}}_d$; λ is a gain for disturbance voltage estimation. Subtracting (29) from (33.1), the following error equation can be obtained.

$$\boldsymbol{e}_s^{k+1} = \boldsymbol{e}_s^k + \frac{T_{sc}}{\hat{L}_g}\left(-\frac{3}{2}(\boldsymbol{e}_u^k + \boldsymbol{u}_o^k)^* \boldsymbol{u}_g^k\right) \tag{34}$$

where $\boldsymbol{e}_s = \hat{\boldsymbol{S}} - \boldsymbol{S}$ is the error of complex power; $\boldsymbol{e}_u = \hat{\boldsymbol{u}}_d - \boldsymbol{u}_d$ is the error of disturbance voltage. It should be noted that actual complex power $\boldsymbol{S}^k$ rather than estimated value $\hat{\boldsymbol{S}}^k$ is used in the last term of (33.1). Such arrangement can cancel $(\hat{R}_g + \omega_g \hat{L}_g J^k)$ related terms in the error equation (34). This can significantly facilitate design process of the observer because J^k is a varying parameter. Setting that the estimation error decays exponentially, i.e.,

$$\boldsymbol{e}_s^{k+1} = (1 - qT_{sc})\boldsymbol{e}_s^k \tag{35}$$

where $q > 0$ is a parameter needs to be designed, the following equation can be derived based on (34) and (35) as

$$\frac{3}{2}(\boldsymbol{e}_u^k + \boldsymbol{u}_o^k)^* \boldsymbol{u}_g^k - \hat{L}_g q \boldsymbol{e}_s^k = 0 \tag{36}$$

Considering the estimation error $\boldsymbol{e}_u^k$ as the disturbance, the control function $\boldsymbol{u}_o^k$ is chosen as

$$\boldsymbol{u}_o^k = \frac{2\hat{L}_g q}{3} \left(\frac{\boldsymbol{e}_s^k}{\boldsymbol{u}_g^k} \right)^*. \tag{37}$$

From (34) and (37), the error dynamics can be obtained as

$$\hat{L}_g \boldsymbol{e}_s^{k+1} = \hat{L}_g \boldsymbol{e}_s^k + T_{sc} \left(-\frac{3}{2}(\boldsymbol{e}_u^k)^* \boldsymbol{u}_g^k - \hat{L}_g q \boldsymbol{e}_s^k \right). \tag{38}$$

According to (38), the following transfer function can be derived.

$$F(z) = \frac{\boldsymbol{e}_s(z)}{\boldsymbol{e}_d(z)} = \frac{3T_{sc}}{2\hat{L}_g} \frac{1}{z - (1 - qT_{sc})} \tag{39}$$

where z is a shift operator and $\boldsymbol{e}_d = -(\boldsymbol{e}_u)^* \boldsymbol{u}_g$. The pole of $F(z)$ is

$$p = 1 - qT_{sc}. \tag{40}$$

To ensure stability, $|p| < 1$ must be satisfied, i.e.,

$$0 < q < \frac{2}{T_{sc}}. \tag{41}$$

Namely, if q satisfies condition (41), estimator of complex power as shown in (33) is stable. In the next subsection, the convergence of the observer will be analyzed and a guideline for selection of q and λ is developed.

B. Analysis of DPDO

First, the relationship between $\hat{\boldsymbol{u}}_d$ and $\boldsymbol{u}_d$ will be analyzed. According to (37) and (39), the following equation can be derived.

$$H(z) = \frac{\boldsymbol{u}_o(z)}{(\boldsymbol{u}_d(z) - \hat{\boldsymbol{u}}_d(z))} = \frac{qT_{sc}}{z - (1 - qT_{sc})} \tag{42}$$

It can be seen that $\boldsymbol{u}_o$ is low pass filtered value of $\boldsymbol{e}_u$. As estimated disturbance voltages $\hat{\boldsymbol{u}}_{dp}$ and $\hat{\boldsymbol{u}}_{dn}$ are reconstructed based on $\boldsymbol{u}_o$, larger q is required for faster dynamic performance. On the other hand, smaller q is preferable for better noise immunity.

From (33.2) and (33.3), $\boldsymbol{u}_o$ can be expressed as

$$\boldsymbol{u}_o(z) = \frac{z - e^{j\omega_g T_{sc}}}{\lambda} \hat{\boldsymbol{u}}_{dp}(z) \tag{43}$$

$$\boldsymbol{u}_o(z) = \frac{z - e^{-j\omega_g T_{sc}}}{\lambda} \hat{\boldsymbol{u}}_{dn}(z) \tag{44}$$

Based on (42) - (44), and considering that $\hat{\boldsymbol{u}}_d = \hat{\boldsymbol{u}}_{dp} + \hat{\boldsymbol{u}}_{dn}$, the relationship between $\hat{\boldsymbol{u}}_d$ and its actual value $\boldsymbol{u}_d$ is given as

$$J(z) = \frac{\hat{\boldsymbol{u}}_d(z)}{\boldsymbol{u}_d(z)} = \frac{2G(z)(z - \cos(\omega_g T_{sc}))}{z^2 + 2\left(G(z) - \cos(\omega_g T_{sc})\right) z + 1 - 2\cos(\omega_g T_{sc}) G(z)} \tag{45}$$

where,

$$G(z) = \frac{\lambda q T_{sc}}{z - (1 - qT_{sc})}. \tag{46}$$

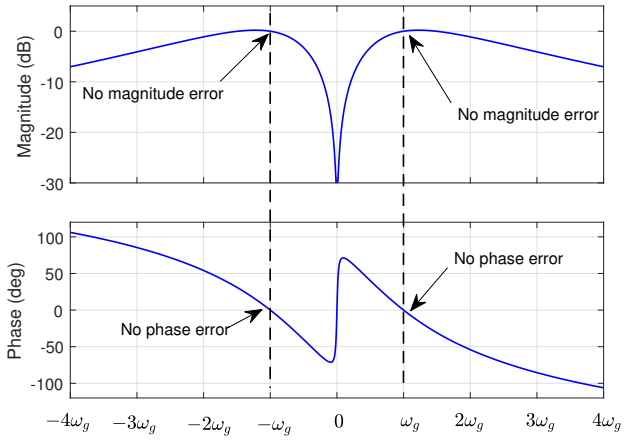

Fig. 1. Bode diagram of $J(z)$.

With a small sampling period, $\cos(\omega_g T_{sc}) \approx 1$. Then, the pole of $J(z)$ can be calculated as

$$p^{1,2} = 1 - \frac{qT_{sc} \pm \sqrt{-qT_{sc}(8\lambda - qT_{sc})}}{2} \tag{47}$$

If

$$8\lambda - qT_{sc} = qT_{sc}, \tag{48}$$

$p^{1,2}$ can be simplified as

$$p^{1,2} = \left(1 - \frac{qT_{sc}}{2}\right) \pm j\frac{qT_{sc}}{2}. \tag{49}$$

According to (49) and considering $e^{-qT_{sc}/2} \approx 1 - {}^{qT_{sc}}/_2$, damping ratio can be set as $\sqrt{2}/2 \approx 0.707$ by satisfying equation (48). The settling time can be subsequently calculated as [33]

$$t_s = \frac{4T_{sc}}{-\ln(1 - qT_{sc}/2)} \approx \frac{8}{q}. \tag{50}$$

Once q is obtained according to the desired settling time t_s, λ can be solved from (48) as

$$\lambda = \frac{qT_{sc}}{4}. \tag{51}$$

Fig. 1 shows the bode diagram of $J(z)$. One can see that, there is no magnitude and phase error at fundamental positive frequency and fundamental negative frequency. Namely, $\hat{\boldsymbol{u}}_d$ could track FPSC and FNSC of $\boldsymbol{u}_d$ accurately. Meanwhile, DC offset and high frequency noises can be suppressed.

Then, estimation error of complex power is analyzed. For a constant $\boldsymbol{e}_d$, final value of $\boldsymbol{e}_s$ can be solved from (39) as

$$\lim_{k\to\infty} \boldsymbol{e}_s^k = \lim_{z\to 1}(1 - z^{-1}) \left(\frac{3T_{sc}}{2\hat{L}_g} \frac{1}{z - (1 - qT_{sc})} \frac{\boldsymbol{e}_d}{1 - z^{-1}}\right) = \frac{3\boldsymbol{e}_d}{2\hat{L}_g q} \tag{52}$$

It has been shown that $\hat{\boldsymbol{u}}_d$ could track $\boldsymbol{u}_d$ without error. Once $\hat{\boldsymbol{u}}_d$ equals $\boldsymbol{u}_d$, $\boldsymbol{e}_d = 0$. According to (52), estimation error of complex power $\boldsymbol{e}_s$ would be finally zero, i.e., estimated complex power can converge to its actual value.

C. Inductance Estimation based On DPDO

As can be seen from (31), a derivative term of complex power related to ΔL exists in $\boldsymbol{u}_d$. Consequently, a large disturbance would occur during transient process, e.g. during step responses. This would lead to deteriorated dynamic performance of DPPC. Hence, it is necessary to estimate ΔL online for better dynamic performance.

According to (21) and (76) derived in the Appendix, $\boldsymbol{u}_d^k$ can be calculated as

$$\boldsymbol{u}_d^k = \frac{2\omega_g \Delta L}{3}\left(\frac{\boldsymbol{S}^k\left(\boldsymbol{u}_g^k/\left(\boldsymbol{u}_g^{'}\right)^k\right)^*}{\boldsymbol{u}_g^k}\right)^* + \frac{2}{3}\Delta R\left(\frac{\boldsymbol{S}^k}{\boldsymbol{u}_g^k}\right)^*. \tag{53}$$

According to (53), multiplying the conjugate of the $\boldsymbol{u}_d^k$ with $\boldsymbol{u}_g^k$ yields the following equation

$$\left(\boldsymbol{u}_d^k\right)^* \boldsymbol{u}_g^k = \frac{2\omega_g \Delta L}{3}\boldsymbol{S}^k\left(\boldsymbol{u}_g^k/\left(\boldsymbol{u}_g^{'}\right)^k\right)^* + \frac{2}{3}\Delta R\boldsymbol{S}^k \tag{54}$$

To calculate the mismatched inductance from (54), ΔR related terms must be eliminated to avoid its influence on the inductance estimation. Considering $\boldsymbol{S}^k \otimes \boldsymbol{S}^k = 0$, the following equation can be easily obtained from (54) as

$$\left(\left(\boldsymbol{u}_d^k\right)^* \boldsymbol{u}_g^k\right) \otimes \boldsymbol{S}^k = \frac{2\omega_g \Delta L}{3}\frac{\left|\boldsymbol{S}^k\right|^2\left(\left(\boldsymbol{u}_g^{'}\right)^k \otimes \boldsymbol{u}_g^k\right)}{\left|\left(\boldsymbol{u}_g^{'}\right)^k\right|^2} \tag{55}$$

Based on (55), ΔL can be directly calculated as

$$\Delta L = \frac{1.5}{\omega_g}\frac{\left|\left(\boldsymbol{u}_g^{'}\right)^k\right|^2 \cdot \left(\left(\boldsymbol{u}_d^k\right)^* \boldsymbol{u}_g^k\right) \otimes \boldsymbol{S}^k}{\left|\boldsymbol{S}^k\right|^2\left(\left(\boldsymbol{u}_g^{'}\right)^k \otimes \boldsymbol{u}_g^k\right)} \tag{56}$$

However, direct calculation is sensitive to measurement noises. In order to obtain a smooth estimation, $\Delta\hat{L}$ can be calculated by integrating ΔL as

$$\begin{aligned}\Delta\hat{L}^{k+1} &= \Delta\hat{L}^k + hT_{sc}\Delta L \\ &= \Delta\hat{L}^k + \frac{1.5hT_{sc}}{\omega_g}\frac{\left|\left(\boldsymbol{u}_g^{'}\right)^k\right|^2 \cdot \left(\left(\boldsymbol{u}_d^k\right)^* \boldsymbol{u}_g^k\right) \otimes \boldsymbol{S}^k}{\left|\boldsymbol{S}^k\right|^2\left(\left(\boldsymbol{u}_g^{'}\right)^k \otimes \boldsymbol{u}_g^k\right)}\end{aligned} \tag{57}$$

where, $h > 0$ is a gain of the integrator. As analyzed in the previous section, $\hat{\boldsymbol{u}}_d^k$ can track $\boldsymbol{u}_d^k$ without error. Therefore, the estimated $\hat{\boldsymbol{u}}_d^k$ from the proposed DPDO is used to replace $\boldsymbol{u}_d^k$ in practical application. With estimation of the mismatched inductance, the estimated inductance $\hat{L}_g$ can be expressed as

$$\hat{L}_g = \hat{L}_0 + \Delta\hat{L}^k \tag{58}$$

where $\hat{L}_0$ is the initialized grid-side inductance in the algorithm, which can be obtained by measurement with a meter or roughly set based on the developer's experience if it is unknown. With the proposed inductance estimation, the mismatch between $\hat{L}_0$ and the actual inductance L_g is online corrected and thus an accurate prior knowledge of grid-side inductance is not required in the proposed method. According to (23) and (58), the mismatched inductance ΔL becomes

$$\Delta L^k = L_g - \hat{L}_0 - \Delta\hat{L}^k. \tag{59}$$

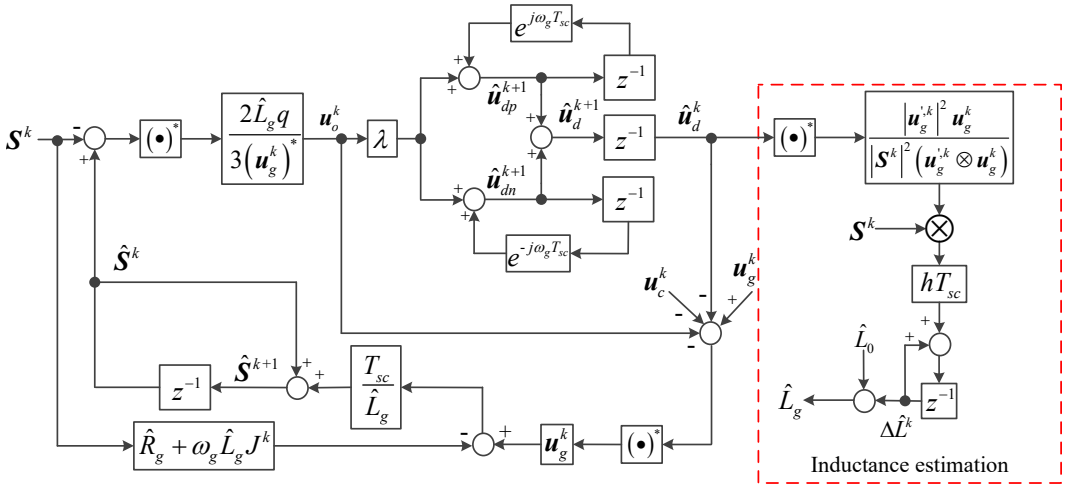

Fig. 2. Block diagram of the proposed DPDO. $(\bullet)^*$ means conjugate of a complex vector and $\otimes$ denotes cross product of two complex vectors.

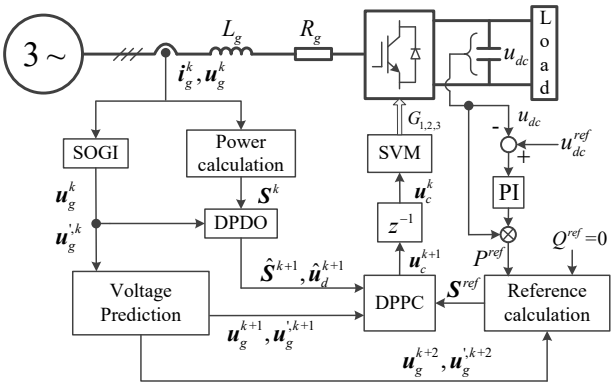

Fig. 3. Control diagram of DPDO based DPPC.

Based on (56), (57) and (59), the relationship between $\Delta\hat{L}$ and $L_g - \hat{L}_0$ can be finally derived as

$$\frac{\Delta\hat{L}}{L_g - \hat{L}_0} = \frac{hT_{sc}}{z - 1 + hT_{sc}}. \tag{60}$$

It is seen that $\Delta\hat{L}$ is the low-pass filtered value of initial estimation error $L_g - \hat{L}_0$. The bandwidth of the low-pass filter is approximately h. Generally, inductance does not vary abruptly in practical applications. A smaller h is preferable for obtaining a smooth $\Delta\hat{L}$. In this paper, h is chosen as 50. Additionally, the incorporation of a low pass filter can ensure the outer loop of inductance estimation works slower than the inner disturbance observer. This helps to decouple the interference between two loops. A complete block diagram of the proposed DPDO is shown in Fig. 2.

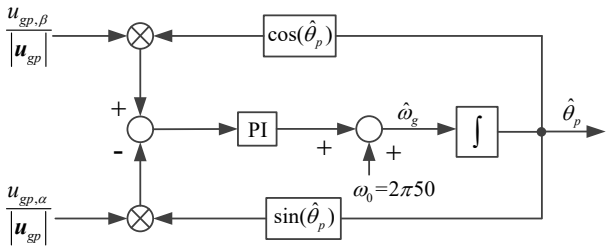

Fig. 4. Control diagram of PLL for online frequency adaption.

V. DPDO BASED ROBUST DPPC

The control diagram of the proposed DPDO based DPPC is shown in Fig. 3. In this paper, only power control performance is concerned and thus the outer DC link voltage control is not discussed here.

Similarly, to make the complex power $\boldsymbol{S}$ reach the reference at the next sampling period, the converter voltage can be solved based on (29) as

$$\boldsymbol{u}_c^k = \boldsymbol{u}_g^k - \frac{2}{3}\left(\frac{(\hat{R}_g - \omega_g \hat{L}_g J^k)\boldsymbol{S}^k}{\boldsymbol{u}_g^k}\right)^* - \frac{2\hat{L}_g}{3T_{sc}}\left(\frac{\boldsymbol{S}^{ref} - \boldsymbol{S}^k}{\boldsymbol{u}_g^k}\right)^* - \boldsymbol{u}_d^k \tag{61}$$

According to (25),

$$\boldsymbol{u}_c^k = \hat{\boldsymbol{u}}_c^k - \boldsymbol{u}_d^k. \tag{62}$$

As $\boldsymbol{u}_d^k$ is unknown, its estimated value $\hat{\boldsymbol{u}}_d^k$ from the DPDO introduced in the previous section is used in (62) to calculate the control voltage. After getting $\boldsymbol{u}_c^k$, SVM is used to generate switching signals to control the rectifier. It is seen from (21) that the calculation of $\boldsymbol{S}^{ref}$ requires quadrature value of grid voltage vector. In this paper, second order generalized integrator (SOGI) is used to get $\boldsymbol{u}_g^{'}$. More details about SOGI can be found in [34] and thus it is not repeated here. After obtaining $\boldsymbol{u}_g^{'}$, the FPSC of grid voltage vector can be calculated as $\boldsymbol{u}_{gp} = 0.5(\boldsymbol{u}_g + j\boldsymbol{u}_g^{'})$. Based on the calculated $\boldsymbol{u}_{gp}$, a standard PLL can be employed for online grid frequency adaption as shown in Fig. 4.

Typically in digital implementation, there is one-step delay between the calculated control voltage and the applied voltage. Similar to [2], [12], [17], the control voltage at $(k+1)$th instant is calculated for delay compensation. By shifting (61) one step ahead, the control voltage $\boldsymbol{u}_c^{k+1}$ can be obtained. It can be seen from (61) that the calculation of $\boldsymbol{u}_c^{k+1}$ requires $\boldsymbol{S}^{k+1}$, $\boldsymbol{u}_d^{k+1}$, $\boldsymbol{u}_g^{k+1}$ and power reference $\boldsymbol{S}^{ref}$ at $(k+2)$th instant. In the following text, the predictions of these variables will be introduced.

$\boldsymbol{u}_g^{k+1}$ can be simply predicted based on (15) as

$$\boldsymbol{u}_g^{k+1} = \boldsymbol{u}_g^k - \omega_g T_{sc}\left(\boldsymbol{u}_g^{'}\right)^k. \tag{63}$$

Similarly, $\left(\boldsymbol{u}_g^{'}\right)^{k+1}$ can be calculated as

$$\left(\boldsymbol{u}_g^{'}\right)^{k+1} = \left(\boldsymbol{u}_g^{'}\right)^k + \omega_g T_{sc}\boldsymbol{u}_g^k. \tag{64}$$

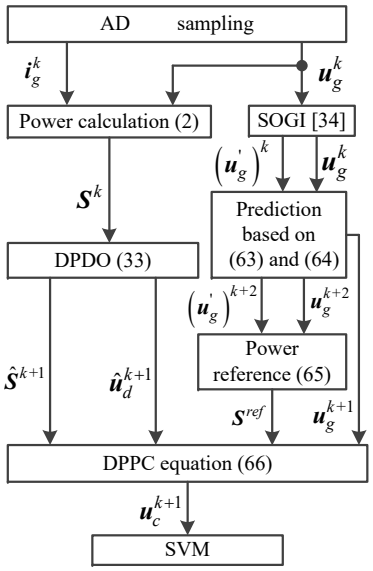

Fig. 5. Schematic diagram of the proposed control method.

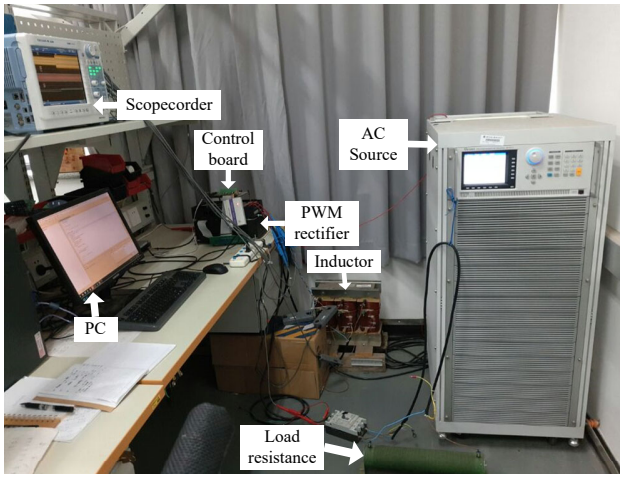

Fig. 6. Experimental test setup.

As can be seen from (33), $\hat{\boldsymbol{S}}^{k+1}$ and $\hat{\boldsymbol{u}}_d^{k+1}$ are directly available in the DPDO. As the designed DPDO can the track actual power accurately despite of mismatched parameters, $\hat{\boldsymbol{S}}^{k+1}$ and $\hat{\boldsymbol{u}}_d^{k+1}$ are employed to replace $\boldsymbol{S}^{k+1}$ and $\boldsymbol{u}_d^{k+1}$ to compensate one-step delay.

For better tracking performance, the complex power reference at $(k+2)$th instant should be predicted in practical application [11]. As seen from (21), $\boldsymbol{u}_g^{k+2}$ and $\left(\boldsymbol{u}_g'\right)^{k+2}$ are required, which can be obtained by further shifting (63) and (64) one-step ahead. Then, $\boldsymbol{S}^{ref}$ can be calculated based on (21) as

$$\boldsymbol{S}^{ref} = jP^{ref}\frac{\left(\left(\boldsymbol{u}_g'\right)^{k+2}\right)^* \boldsymbol{u}_g^{k+2}}{\boldsymbol{u}_g^{k+2} \otimes \left(\boldsymbol{u}_g'\right)^{k+2}} \tag{65}$$

Finally, the control voltage $\boldsymbol{u}_c^{k+1}$ with delay compensation can be expressed as

$$\boldsymbol{u}_c^{k+1} = \boldsymbol{u}_g^{k+1} - \frac{2}{3}\left(\frac{(\hat{R}_g - \omega_g \hat{L}_g J^{k+1})\hat{\boldsymbol{S}}^{k+1}}{\boldsymbol{u}_g^{k+1}}\right)^* - \frac{2\hat{L}_g}{3T_{sc}}\left(\frac{\boldsymbol{S}^{ref} - \hat{\boldsymbol{S}}^{k+1}}{\boldsymbol{u}_g^{k+1}}\right)^* - \hat{\boldsymbol{u}}_d^{k+1}. \tag{66}$$

It should be noted that for a conventional deadbeat predictive power control under unbalanced grid conditions, the predictions of $\boldsymbol{S}^{k+1}$, $\boldsymbol{u}_g^{k+1}$ and $\boldsymbol{S}^{ref}$ at $(k+2)$th instant are also required to compensate for one-step delay. The difference is that in conventional methods, the complex power $\boldsymbol{S}^{k+1}$ is directly predicted based on the estimated system model (29). This will result in errors when there are model mismatches. While in this paper, the complex power at $(k+1)$th instant is obtained by a closed-loop DPDO as shown in (33), which can provide accurate predictions even with model uncertainties. Since delay compensation and disturbance estimation are integrated together, the complexity is not substantially increased compared with conventional deadbeat predictive power control, as also confirmed by the comparison of execution time shown in the next section. A schematic diagram of the proposed control algorithm is shown in Fig. 5.

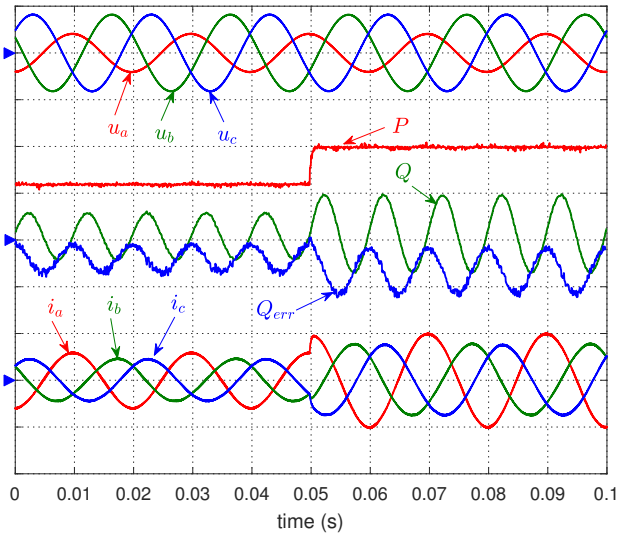

Fig. 7. Experimental results of prior DPPC when $\hat{L}_g = 0.5L_g$. u_{abc}: 150 V/div, P: 500 W/div, Q: 500 Var/div, Q_{err}: 100 Var/div, i_{abc} : 8 A/div.

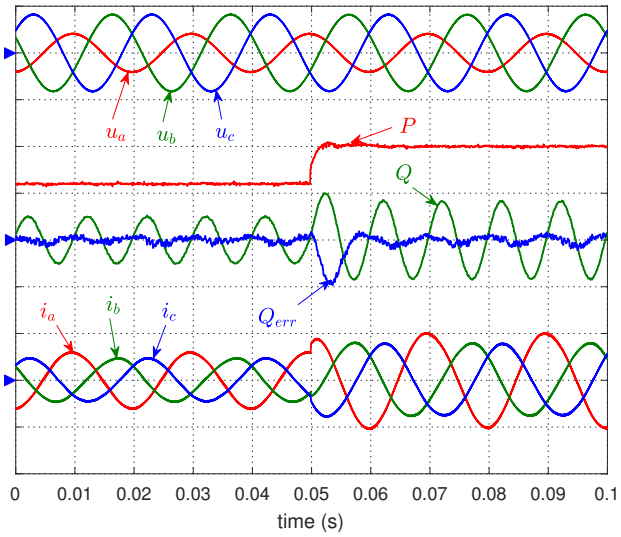

Fig. 8. Experimental results of DPDO based DPPC without ΔL adaptation when $\hat{L}_0 = 0.5L_g$. u_{abc}: 150 V/div, P: 500 W/div, Q: 500 Var/div, Q_{err}: 100 Var/div, i_{abc} : 8 A/div.

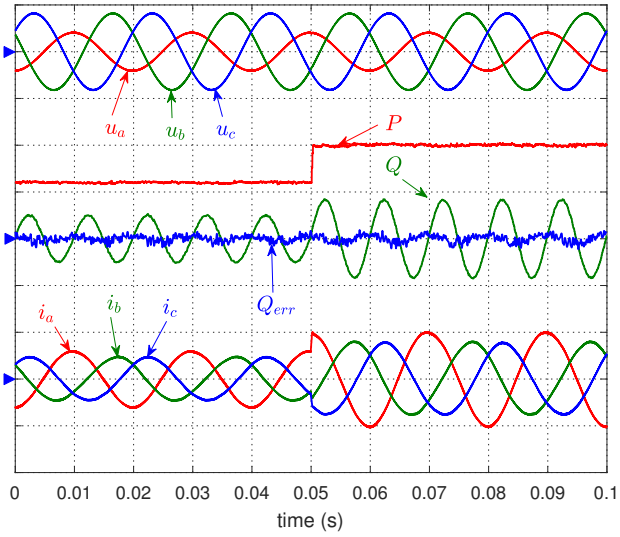

Fig. 9. Experimental results of DPDO based DPPC with ΔL adaptation when $\hat{L}_0 = 0.5L_g$. u_{abc}: 150 V/div, P: 500 W/div, Q: 500 Var/div, Q_{err}: 100 Var/div, i_{abc} : 8 A/div.

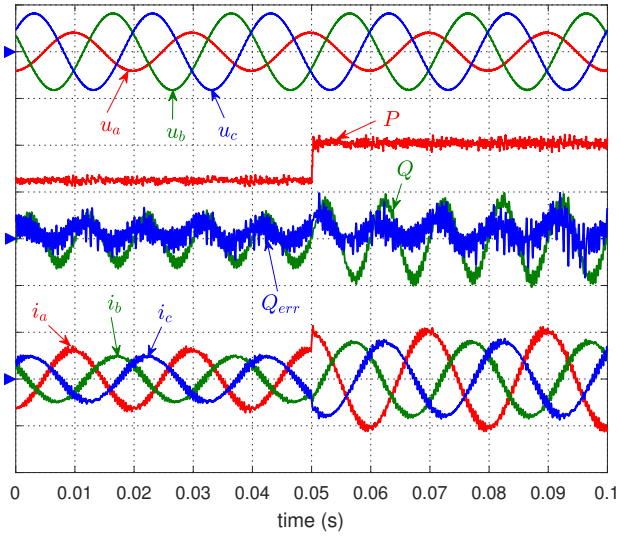

Fig. 10. Experimental results of prior DPPC when $\hat{L}_g = 2L_g$. u_{abc}: 150 V/div, P: 500 W/div, Q: 500 Var/div, Q_{err}: 200 Var/div, i_{abc} : 8 A/div.

VI. Experimental Results

Experimental tests on a two-level VSR were performed to verify the effectiveness of the proposed method. The system and control parameters are listed in Table I. The per-unit values are calculated with power base and voltage base selected as 1 kVA and 150 V respectively. A 32-bit DSP TMS320F28335 is used to implement the whole algorithm. Experimental data is sampled by a scopecorder DL850. Chroma 61511, a programmable AC source, is used to provide unbalanced grid conditions. The whole experimental setup is shown in Fig. 6. A prior method

TABLE I

SYSTEM AND CONTROL PARAMETERS

System Parameters	Symbol	Value	p.u. value
Line resistance	R_g	0.3 Ω	0.0077
Line inductance	L_g	10 mH	0.0806
Line-line voltage	U_N	150 V	1
DC-link capacitor	C	840 μF	10.2842
Line voltage frequency	f_g	50 Hz	1
Load resistance	R_L	100 Ω	2.566
Sampling period	T_{sc}	100 μs	0.005
DPDO parameter 1	q	2000	N/A
DPDO parameter 2	λ	0.05	N/A

presented in [18], which is named as prior DPPC in the following text, was also carried out for comparison. On the laboratory test rig, it takes 39.27 μs and 43.73 μs to execute algorithms of the prior DPPC and the proposed DPPC respectively. Compared with the prior DPPC, the execution time is only increased by 4.46 μs, suggesting that the complexity is not substantially increased by incorporating the proposed disturbance observer and online inductance adaption. Considering the limitation of the execution time, the sampling frequency must be set below $1/43.73\mu$s ≈ 22.8 kHz. In all the following experimental tests, the sampling frequency and switching frequency are set as 10 kHz in order to obtain satisfactory performance with acceptable switching losses and sufficient time for executing the control algorithm. For the studied PWM rectifier, the minimum DC-link voltage should be larger than the peak value of line-line grid voltage. As shown in the Table I, the peak line-line voltage for our test rig is $150\sqrt{2} \approx 212$ V. Considering the load resistance is 100 Ω, the active power reference should be no smaller than $212^2/100 = 450$ W. Additionally, due to the limitation of the rated current, the active power reference is set below 1000 W. To avoid the influence of outer DC voltage control loop on the inner power control, experimental tests were initially carried out by disconnecting outer PI controller and the rectifier works in power control mode. After verifying the superiority of the proposed DPPC, the voltage control mode is tested and the closed-loop DC voltage regulation is verified with step change in DC load.

Figs. 7-9 show the comparative results when the initial estimated inductance $\hat{L}_0$ is half of the actual value. Initially, P^{ref} is 600 W and then steps to 1000 W. And, 50% voltage dip in phase-A is applied during the whole experimental tests. In the figure, Q_{err} is the tracking error of reactive power. It is seen that both methods can achieve constant active power and sinusoidal grid currents under unbalanced grid conditions. However, the prior DPPC is sensitive to the grid-side inductance mismatch, as analyzed in the Section III-B. From Fig. 7, one can see that there is a significant deviation of reactive power for the prior DPPC. While from Fig. 8, it is seen that Q_{err} is around zero during steady state for the DPDO based DPPC. Though steady-state tracking accuracy is improved with DPDO, existence of ΔL will result in deteriorated dynamic performance as analyzed previously. It can be seen in Fig. 8 that there is larger tracking error of reactive power and slower tracking performance of active power during the transient process. Fig. 9 shows test results when ΔL is adapted online. The undesired transient responses

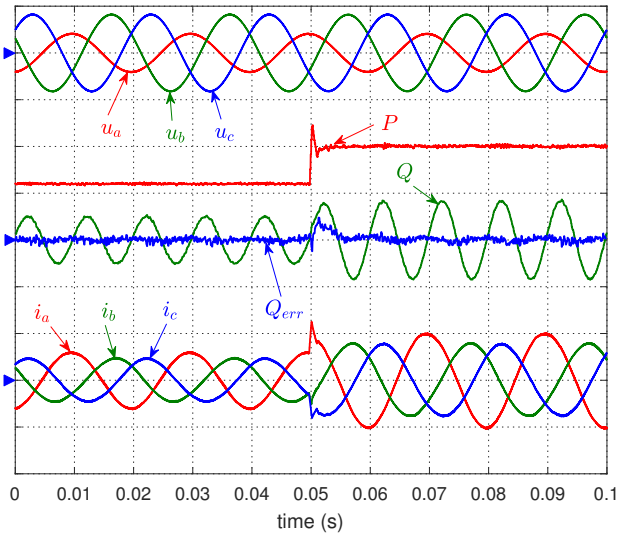

Fig. 11. Experimental results of DPDO based DPPC without ΔL adaptation when $\hat{L}_0 = 2L_g$. u_{abc}: 150 V/div, P: 500 W/div, Q: 500 Var/div, Q_{err}: 100 Var/div, i_{abc} : 8 A/div.

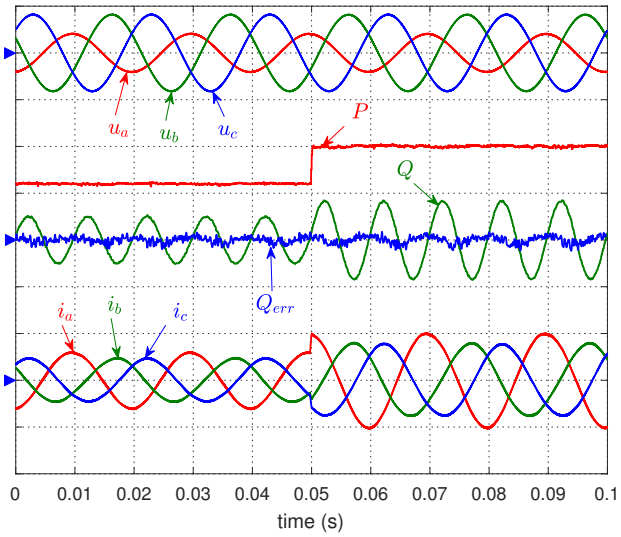

Fig. 12. Experimental results of DPDO based DPPC with ΔL adaptation when $\hat{L}_0 = 2L_g$. u_{abc}: 150 V/div, P: 500 W/div, Q: 500 Var/div, Q_{err}: 100 Var/div, i_{abc} : 8 A/div.

shown in Fig. 8 does not exist when ΔL adaption is enabled. These tests confirm that the proposed DPDO can improve tracking accuracy of DPPC under parameter mismatches. Further improvement can be made by online adaptation of inductance. Apparently, DPDO based DPPC with online inductance estimation presents best overall performance in this test.

Under the same conditions as previous tests, Figs. 10-12 illustrate comparative results when the initial estimated inductance $\hat{L}_0$ is twice of the actual value. For prior DPPC as shown in Fig. 10, significant ripple components can be observed in the recorded power and current waveforms, indicating the control system is poorly damped in this test case. For DPDO based DPPC without inductance estimation as shown in Fig. 11, the steady-state waveforms are smooth without harmonic components. And, the average tracking error, Q_{err}, is zero. This test further confirms that DPDO can eliminate steady-state tracking error in the DPPC when inductance mismatch exists. However, large overshoot can be seen in P^{ref} step responses. By contrast, when ΔL adaptation is enabled, DPDO based DPPC shows superior performance over prior DPPC and DPPC with only DPDO, as can be seen from the results shown in Fig. 12.

According to the above tests, it can be concluded that DPDO based DPPC with ΔL adaptation has best performance among three methods. In the following two tests, the influence of resistance error ΔR will be evaluated. From analysis in [12], it can be seen that larger $\hat{R}_g$ with smaller $\hat{L}_0$, and smaller $\hat{R}_g$ with larger $\hat{L}_0$ can result in the worst working conditions. Hence, these two test cases were performed to verify the effectiveness of the proposed method. The results are shown in Figs. 13 and 14. It is seen that Q_{err} is nearly zero. Actual power P can track P^{ref} quickly with no significant overshoot during transient process for both test cases.

Figs. 15-17 present responses of the proposed DPDO based DPPC under two-phase voltage sag, three-phase voltage sag and one-phase deep voltage sag conditions respectively. In these tests, $P^{ref} = 600$ W. With ideal grid

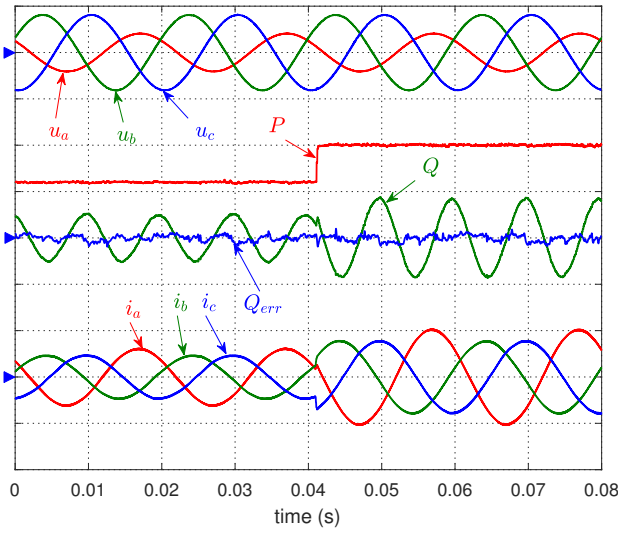

Fig. 13. Experimental results of DPDO based DPPC with ΔL adaptation when $\hat{R}_g = 2R_g$ and $\hat{L}_0 = 0.5L_g$. u_{abc}: 150 V/div, P: 500 W/div, Q: 500 Var/div, Q_{err}: 100 Var/div, i_{abc} : 8 A/div.

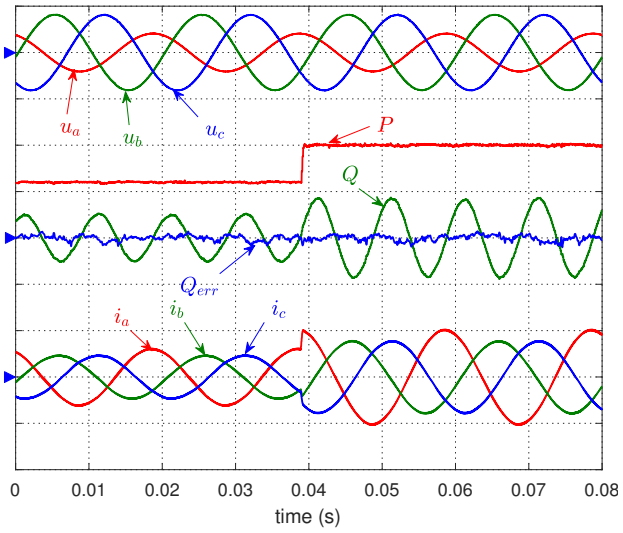

Fig. 14. Experimental results of DPDO based DPPC with ΔL adaptation when $\hat{R}_g = 0.5R_g$ and $\hat{L}_0 = 2L_g$. u_{abc}: 150 V/div, P: 500 W/div, Q: 500 Var/div, Q_{err}: 100 Var/div, i_{abc} : 8 A/div.

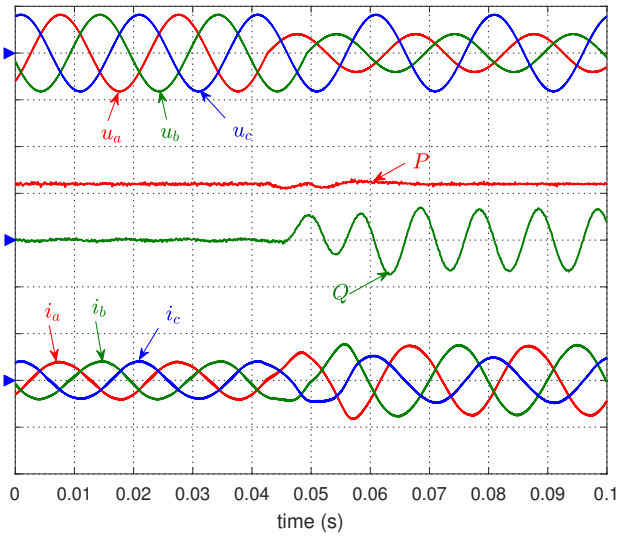

Fig. 15. Experimental results of DPDO based DPPC with ΔL adaptation when 50% voltage dips in phase-A and phase-B are applied. u_{abc}: 150 V/div, P: 500 W/div, Q: 500 Var/div, i_{abc} : 8 A/div.

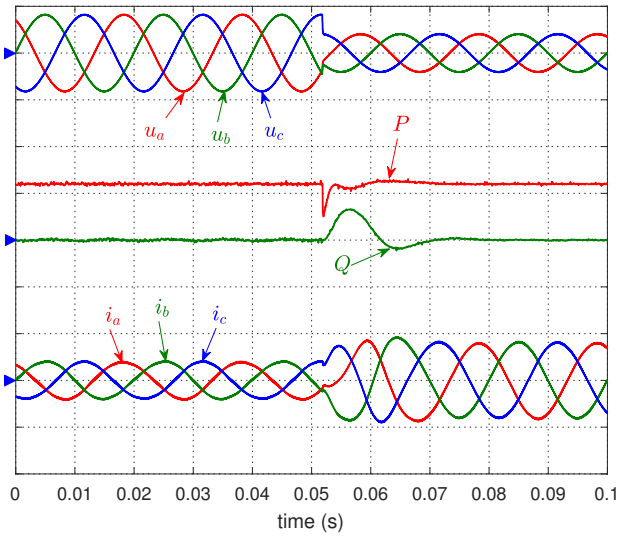

Fig. 16. Experimental results of DPDO based DPPC with ΔL adaptation when 50% voltage dips in three phases are suddenly applied. u_{abc}: 150 V/div, P: 500 W/div, Q: 500 Var/div, i_{abc} : 8 A/div.

voltages, it is seen that both active power and reactive power are kept constant at their references and three-phase grid currents are balanced and sinusoidal. After voltage dip, active power P can return to its reference quickly and twice of grid frequency oscillations can be observed in the reactive power when grid voltages are unbalanced. However, shapes of grid currents are still sinusoidal. Additionally, there is no inrush current when voltage sag suddenly occurs. The steady-state results are in accordance with that presented in [18], [31]. These tests confirm that the proposed method can properly work under both ideal and severely unbalanced grid conditions.

The effectiveness of inductance estimation was also evaluated. Fig. 18 shows the estimated $\hat{L}_g$ when there is 50%

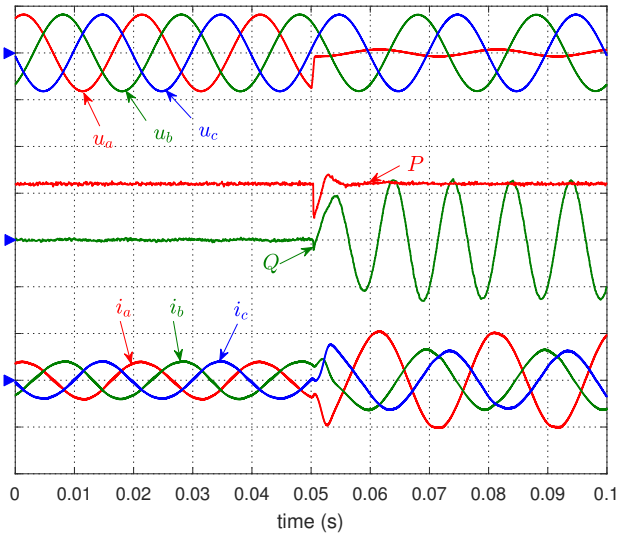

Fig. 17. Experimental results of DPDO based DPPC with ΔL adaptation when 90% voltage dip in phase-A is suddenly applied. u_{abc}: 150 V/div, P: 500 W/div, Q: 500 Var/div, i_{abc} : 8 A/div.

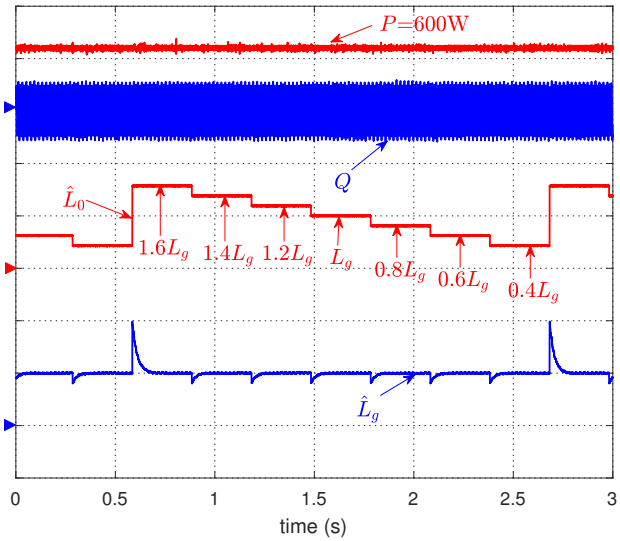

Fig. 18. Experimental results of DPDO based DPPC with ΔL adaptation when $\hat{L}_0$ varies from $1.6L_g$ to $0.4L_g$ under unbalanced grid condition. P: 500 W/div, Q: 500 Var/div, $\hat{L}_0$: 10 mH/div, $\hat{L}_g$: 10 mH/div.

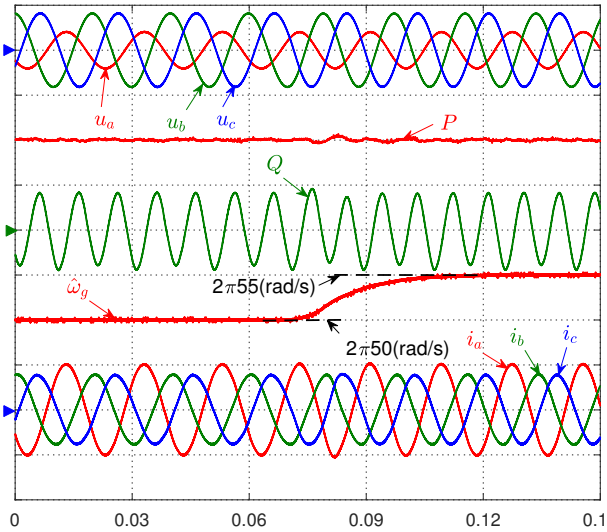

Fig. 19. Experimental results of the proposed DPPC with step frequency change of +5 Hz under unbalanced grid conditions. u_{abc}: 150 V/div, P: 500 W/div, Q: 500 Var/div, $\hat{\omega}_g$: $2\pi5$ (rad/s)/div, i_{abc} : 8 A/div.

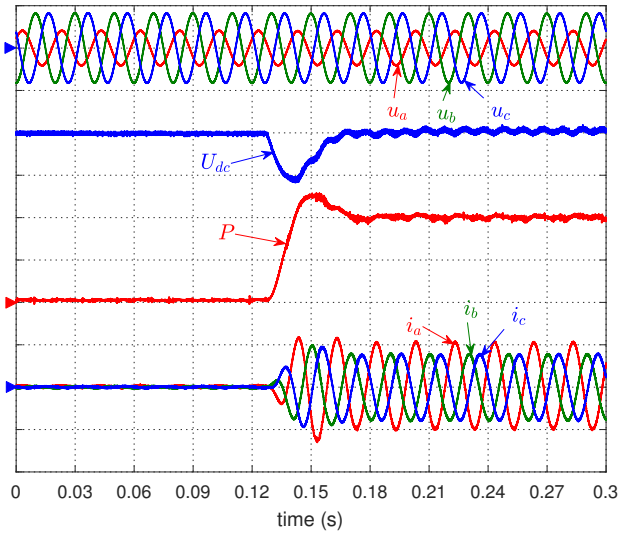

Fig. 20. Responses of DC-link voltage when external DC load is suddenly applied under unbalanced grid conditions.U_{dc}^{ref}: 300 V, u_{abc}: 150 V/div, P: 500 W/div, U_{dc}: 20 V/div, i_{abc} : 8 A/div.

voltage dip in phase-A. During experimental tests, the real inductance is not changed but $\hat{L}_0$ is deliberately varied from $1.6L_g$ to $0.4L_g$. It can be found that $\hat{L}_g$ always converges to its actual value when $\hat{L}_0$ changes, indicating that the developed inductance adaptive scheme works well with different inductance errors.

Fig. 19 illustrates the experimental results when +5 Hz sudden grid frequency change is applied under unbalanced grid conditions. When grid frequency suddenly changes, there are some transient oscillations in both active power and reactive power. However, the system is stable and there is no inrush current. As the estimated grid frequency

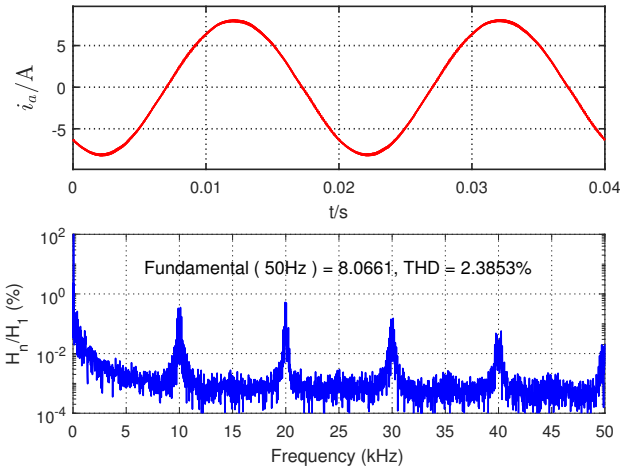

Fig. 21. Harmonic spectrum of phase current for the proposed DPPC.

gradually converges to its actual value with the implemented PLL, the whole system can return to its normal operation after sudden frequency change.

Finally, the effectiveness of the proposed DPPC is tested with closed-loop DC-link voltage regulation. In this test, the active power reference is generated by the outer PI controller as shown in Fig. 3. The results when the external DC load is suddenly applied are depicted in Fig. 20. It can be found that when the external load is suddenly applied, the DC voltage can quickly return to its reference (300 V) after a drop. Although grid voltages are unbalanced, the active power is almost constant during steady state and three-phase currents are sinusoidal. Due to the influence of the unbalanced grid voltages, there are minor oscillations at twice grid frequency in the DC-link voltage. To eliminate DC voltage oscillations, control objective aiming at constant converter-side active power, as shown in [35], can be selected. However, there would be significant power ripples at input-terminals. As this part is not the major concern of this paper, it will not be further expanded and more details can be found in [35]. Harmonic spectrum of the obtained phase current during steady-state operation is shown in Fig. 21. The current total harmonic distortion (THD) is about 2.39%. Due to the use of SVM, high-order harmonics are mainly concentrated around multiplies of switching frequency (10 kHz).

VII. Conclusion

In this paper, a DPDO based DPPC is proposed and experimentally verified with considerations of mismatched model parameters and unbalanced grid voltages. The designed DPDO can accurately estimate disturbance resulting from mismatched parameters. Stability and convergence as well as parameter tuning are theoretically analyzed. The DPDO is designed in discrete-time domain, facilitating direct implementation in a digital controller. Due to predictive ability of DPDO, delay compensation and disturbance estimation is simultaneously achieved. As a result, tracking accuracy can be improved with mismatched parameters without significantly complicating implementation when compared with a standard DPPC. To further improve dynamic performance, an inductance adaptation scheme is developed, which can accurately estimate mismatched inductance with different initial errors. Experimental results

and comparative studies validate that the DPDO based DPPC with inductance estimation could achieve satisfactory steady-state and dynamic performance under different parameter mismatches.

APPENDIX

During steady-state operation, $\boldsymbol{S}^k = \boldsymbol{S}^{ref}$. According to (20), the following equation can be derived.

$$\boldsymbol{S}^{k+1} - \boldsymbol{S}^k = jP\left(\frac{\boldsymbol{u}_g^{k+1} \odot \boldsymbol{u}_g^{q,k+1}}{\boldsymbol{u}_g^{k+1} \otimes \boldsymbol{u}_g^{q,k+1}} - \frac{\boldsymbol{u}_g^{k} \odot \boldsymbol{u}_g^{q,k}}{\boldsymbol{u}_g^{k} \otimes \boldsymbol{u}_g^{q,k}}\right) \tag{67}$$

For two complex vectors A and B, $A \otimes jB = A \odot B$. Hence, $\boldsymbol{u}_g \otimes \boldsymbol{u}_g^q$ and $\boldsymbol{u}_g \odot \boldsymbol{u}_g^q$ can be expanded in terms of $\boldsymbol{u}_{gp}$ and $\boldsymbol{u}_{gn}$ as

$$\boldsymbol{u}_g \otimes \boldsymbol{u}_g^q = (\boldsymbol{u}_{gp} + \boldsymbol{u}_{gn}) \otimes (-j\boldsymbol{u}_{gp} + j\boldsymbol{u}_{gn}) \tag{68}$$

$$= |\boldsymbol{u}_{gn}|^2 - |\boldsymbol{u}_{gp}|^2, \tag{69}$$

$$\boldsymbol{u}_g \odot \boldsymbol{u}_g^q = (\boldsymbol{u}_{gp} + \boldsymbol{u}_{gn}) \odot (-j\boldsymbol{u}_{gp} + j\boldsymbol{u}_{gn}) \tag{70}$$

$$= 2\boldsymbol{u}_{gn} \otimes \boldsymbol{u}_{gp}. \tag{71}$$

It can be seen that $\boldsymbol{u}_g \otimes \boldsymbol{u}_g^q$ is a constant during steady state operation. In the following text, variable M is used to replace $\boldsymbol{u}_g \otimes \boldsymbol{u}_g^q$ for simplicity, i.e.,

$$M = \boldsymbol{u}_g \otimes \boldsymbol{u}_g^q = |\boldsymbol{u}_{gn}|^2 - |\boldsymbol{u}_{gp}|^2 \tag{72}$$

(67) can then be rewritten as

$$\boldsymbol{S}^{k+1} - \boldsymbol{S}^k = \frac{2jP\left[\left(\boldsymbol{u}_{gn}^{k+1} \otimes \boldsymbol{u}_{gp}^{k+1}\right) - \left(\boldsymbol{u}_{gn}^{k} \otimes \boldsymbol{u}_{gp}^{k}\right)\right]}{M}. \tag{73}$$

With a small sampling period, $\boldsymbol{u}_{gn}^{k+1} = \boldsymbol{u}_{gn}^{k}\left(1 - j\omega_g T_{sc}\right)$ and $\boldsymbol{u}_{gp}^{k+1} = \boldsymbol{u}_{gp}^{k}\left(1 + j\omega_g T_{sc}\right)$. Neglecting T_{sc}^2 related terms, (73) can be simplified as

$$\boldsymbol{S}^{k+1} - \boldsymbol{S}^k = jPT_{sc}\frac{4\omega_g \boldsymbol{u}_{gp}^{k} \odot \boldsymbol{u}_{gn}^{k}}{M}. \tag{74}$$

According to (21) and (69),

$$J^k \omega_g \boldsymbol{S}^k = jP^{ref}\frac{\omega_g \left|\boldsymbol{u}_g^{q,k}\right|^2}{M} = j\omega_g P\frac{\left|\boldsymbol{u}_{gn}^{k}\right|^2 + \left|\boldsymbol{u}_{gp}^{k}\right|^2 - 2\boldsymbol{u}_{gp}^{k} \odot \boldsymbol{u}_{gn}^{k}}{M}. \tag{75}$$

Based on (74) and (75), (31) can be rewritten as

$$\boldsymbol{u}_d^k = \frac{2\omega_g \Delta L}{3}\left(\frac{jP\left|\boldsymbol{u}_g^k\right|^2}{M\boldsymbol{u}_g^k}\right)^* + \frac{2}{3}\Delta R\left(\frac{\boldsymbol{S}^k}{\boldsymbol{u}_g^k}\right)^*. \tag{76}$$

From (21),

$$\left(\frac{\boldsymbol{S}^k}{\boldsymbol{u}_g^k}\right)^* = -jP\left(\frac{j\boldsymbol{u}_{gn} - j\boldsymbol{u}_{gp}}{M}\right)$$

and considering $\left|\boldsymbol{u}_g^k\right|^2 = \left(\boldsymbol{u}_g^k\right)^* \boldsymbol{u}_g^k$, (76) can then be rearranged as

$$\begin{aligned}\boldsymbol{u}_d^k &= \frac{2}{3}P\frac{j\omega_g \Delta L\left(\boldsymbol{u}_{gp} + \boldsymbol{u}_{gn}\right) + \Delta R\left(\boldsymbol{u}_{gp} - \boldsymbol{u}_{gn}\right)}{M} \\ &= \frac{2P\left[\left(j\omega_g \Delta L + \Delta R\right)\boldsymbol{u}_{gp} + \left(j\omega_g \Delta L - \Delta R\right)\boldsymbol{u}_{gn}\right]}{3M}.\end{aligned} \tag{77}$$

It is clear that $\boldsymbol{u}_d^k$ consists of the following FPSC $\boldsymbol{u}_{dp}^k$ and FNSC $\boldsymbol{u}_{dn}^k$ as

$$\boldsymbol{u}_{dp}^k = \frac{2P\left(j\omega_g \Delta L + \Delta R\right)}{3M}\boldsymbol{u}_{gp}, \tag{78}$$

$$\boldsymbol{u}_{dn}^k = \frac{2P\left(j\omega_g \Delta L - \Delta R\right)}{3M}\boldsymbol{u}_{gn}. \tag{79}$$

REFERENCES

[1] S. Vazquez, J. I. Leon, L. G. Franquelo, J. Rodriguez, H. A. Young, A. Marquez, and P. Zanchetta, "Model predictive control: A review of its applications in power electronics," *IEEE Ind. Electron. Mag.*, vol. 8, no. 1, pp. 16–31, March 2014.

[2] Y. Zhang, J. Gao, and C. Qu, "Relationship between two direct power control methods for PWM rectifiers under unbalanced network," *IEEE Trans. Power Electron.*, vol. 32, no. 5, pp. 4084–4094, May 2017.

[3] V. Blasko and V. Kaura, "A new mathematical model and control of a three-phase AC-DC voltage source converter," *IEEE Trans. Power Electron.*, vol. 12, no. 1, pp. 116–123, Jan 1997.

[4] Z. Yingchao, Z. Zhengming, Z. Yongchang, L. Ting, and Y. Liqiang, "The virtual flux oriented control of three-level neutral point clamped pwm rectifier," in *2007 International Conference on Electrical Machines and Systems (ICEMS)*, Oct 2007, pp. 22–27.

[5] Y. Zhang and C. Qu, "Table-based direct power control for three-phase AC/DC converters under unbalanced grid voltages," *IEEE Trans. Power Electron.*, vol. 30, no. 12, pp. 7090–7099, Dec 2015.

[6] A. M. Razali, M. A. Rahman, G. George, and N. A. Rahim, "Analysis and design of new switching lookup table for virtual flux direct power control of grid-connected three-phase PWM AC - DC converter," *IEEE Trans. Ind. Appl.*, vol. 51, no. 2, pp. 1189–1200, March 2015.

[7] Y. Zhang and W. Xie, "Low complexity model predictive control-single vector-based approach," *IEEE Trans. Power Electron.*, vol. 29, no. 10, pp. 5532–5541, Oct 2014.

[8] J. Rodriguez, M. Kazmierkowski, J. Espinoza, P. Zanchetta, H. Abu-Rub, H. Young, and C. Rojas, "State of the art of finite control set model predictive control in power electronics," *IEEE Trans. Ind. Informat.*, vol. 9, no. 2, pp. 1003–1016, 2013.

[9] A. G. Yepes, A. Vidal, J. Malvar, O. Lòpez, and J. Doval-Gandoy, "Tuning method aimed at optimized settling time and overshoot for synchronous proportional-integral current control in electric machines," *IEEE Trans. Power Electron.*, vol. 29, no. 6, pp. 3041–3054, June 2014.

[10] A. Bouafia, J. P. Gaubert, and F. Krim, "Predictive direct power control of three-phase pulsewidth modulation (PWM) rectifier using space-vector modulation (SVM)," *IEEE Trans. Power Electron.*, vol. 25, no. 1, pp. 228–236, Jan 2010.

[11] J. Rodriguez and P. Cortes, *Predictive control of power converters and electrical drives*. Wiley-IEEE Press, 2012, vol. 37.

[12] H. A. Young, M. A. Perez, and J. Rodriguez, "Analysis of finite-control-set model predictive current control with model parameter mismatch in a three-phase inverter," *IEEE Trans. Ind. Electron.*, vol. 63, no. 5, pp. 3100–3107, May 2016.

[13] C. Xia, M. Wang, Z. Song, and T. Liu, "Robust model predictive current control of three-phase voltage source PWM rectifier with online disturbance observation," *IEEE Trans. Ind. Informat.*, vol. 8, no. 3, pp. 459–471, Aug 2012.

[14] Z. Song, Y. Tian, W. Chen, Z. Zou, and Z. Chen, "Predictive duty cycle control of three-phase active-front-end rectifiers," *IEEE Trans. Power Electron.*, vol. 31, no. 1, pp. 698–710, Jan 2016.

[15] J. S. Lee and R. D. Lorenz, "Robustness analysis of deadbeat-direct torque and flux control for IPMSM drives," *IEEE Trans. Ind. Electron.*, vol. 63, no. 5, pp. 2775–2784, May 2016.

[16] W. Xie, X. Wang, F. Wang, W. Xu, R. M. Kennel, D. Gerling, and R. D. Lorenz, "Finite-control-set model predictive torque control with a deadbeat solution for PMSM drives," *IEEE Trans. Ind. Electron.*, vol. 62, no. 9, pp. 5402–5410, Sept 2015.

[17] W. Song, J. Ma, L. Zhou, and X. Feng, "Deadbeat predictive power control of single-phase three-level neutral-point-clamped converters using space-vector modulation for electric railway traction," *IEEE Trans. Power Electron.*, vol. 31, no. 1, pp. 721–732, Jan 2016.

[18] Y. Zhang and C. Qu, "Direct power control of a pulse width modulation rectifier using space vector modulation under unbalanced grid voltages," *IEEE Trans. Power Electron.*, vol. 30, no. 10, pp. 5892–5901, Oct 2015.

[19] S. Kwak, U. C. Moon, and J. C. Park, "Predictive-control-based direct power control with an adaptive parameter identification technique for improved AFE performance," *IEEE Trans. Power Electron.*, vol. 29, no. 11, pp. 6178–6187, Nov 2014.

[20] B. Arif, L. Tarisciotti, P. Zanchetta, J. C. Clare, and M. Degano, "Grid parameter estimation using model predictive direct power control," *IEEE Trans. Ind. Appl.*, vol. 51, no. 6, pp. 4614–4622, Nov 2015.

[21] W. Song, Z. Deng, S. Wang, and X. Feng, "A simple model predictive power control strategy for single-phase pwm converters with modulation function optimization," *IEEE Trans. Power Electron.*, vol. 31, no. 7, pp. 5279–5289, July 2016.

[22] D. Martin and E. Santi, "Autotuning of digital deadbeat current controllers for grid-tie inverters using wide bandwidth impedance identification," *IEEE Trans. Ind. Appl.*, vol. 50, no. 1, pp. 441–451, Jan 2014.

[23] S. K. Kim, D. K. Choi, K. B. Lee, and Y. I. Lee, "Offset-free model predictive control for the power control of three-phase AC/DC converters," *IEEE Trans. Ind. Electron.*, vol. 62, no. 11, pp. 7114–7126, Nov 2015.

[24] S. K. Kim, "Offset-free one-step ahead state predictor for power electronic applications using robust proportional-integral observer," *IEEE Trans. Ind. Electron.*, vol. 63, no. 3, pp. 1763–1770, March 2016.

[25] K. J. Lee, B. G. Park, R. Y. Kim, and D. S. Hyun, "Robust predictive current controller based on a disturbance estimator in a three-phase grid-connected inverter," *IEEE Trans. Power Electron.*, vol. 27, no. 1, pp. 276–283, Jan 2012.

[26] X. Zhang, B. Hou, and Y. Mei, "Deadbeat predictive current control of permanent-magnet synchronous motors with stator current and disturbance observer," *IEEE Trans. Power Electron.*, vol. 32, no. 5, pp. 3818–3834, May 2017.

[27] Z. Dai and W. Lin, "Adaptive estimation of three-phase grid voltage parameters under unbalanced faults and harmonic disturbances," *IEEE Trans. Power Electron.*, vol. 32, no. 7, pp. 5613–5627, July 2017.

[28] J. R. Fischer, S. A. González, I. Carugati, M. A. Herrán, M. G. Judewicz, and D. O. Carrica, "Robust predictive control of grid-tied converters based on direct power control," *IEEE Trans. Power Electron.*, vol. 29, no. 10, pp. 5634–5643, Oct 2014.

[29] K. Lee, T. M. Jahns, T. A. Lipo, and V. Blasko, "New control method including state observer of voltage unbalance for grid voltage-source converters," *IEEE Trans. Ind. Electron.*, vol. 57, no. 6, pp. 2054–2065, June 2010.

[30] Y. Suh and T. A. Lipo, "Control scheme in hybrid synchronous stationary frame for pwm ac/dc converter under generalized unbalanced operating conditions," *IEEE Trans. Ind. Appl.*, vol. 42, no. 3, pp. 825–835, May 2006.

[31] K. Ma, W. Chen, M. Liserre, and F. Blaabjerg, "Power controllability of a three-phase converter with an unbalanced ac source," *IEEE Trans. Power Electron.*, vol. 30, no. 3, pp. 1591–1604, March 2015.

[32] H. Yang, Y. Zhang, J. Liang, N. Zhang, and P. Walker, "A robust deadbeat predictive power control with sliding mode disturbance observer for PWM rectifiers," in *IEEE Energy Conversion Congr. and Expo.*, Cincinnati, OH., OCT 2017, pp. 4595–4600.

[33] K. Ogata, *Discrete-time control systems*. Prentice Hall Englewood Cliffs, NJ, 1995, vol. 2.

[34] P. Rodríguez, A. Luna, R. S. M. noz Aguilar, I. Etxeberria-Otadui, R. Teodorescu, and F. Blaabjerg, "A stationary reference frame grid synchronization system for three-phase grid-connected power converters under adverse grid conditions," *IEEE Trans. Power Electron.*, vol. 27, no. 1, pp. 99–112, Jan 2012.

[35] Z. Li, Y. Li, P. Wang, H. Zhu, C. Liu, and W. Xu, "Control of three-phase boost-type pwm rectifier in stationary frame under unbalanced input voltage," *IEEE Trans. Power Electron.*, vol. 25, no. 10, pp. 2521–2530, Oct 2010.